

# Bioinspired Fabrication of Superhydrophobic Graphene Films by Two-Beam Laser Interference

Hao-Bo Jiang, Yong-Lai Zhang,\* Dong-Dong Han, Hong Xia, Jing Feng, Qi-Dai Chen, Zi-Ruo Hong, and Hong-Bo Sun\*

Reported here is a bioinspired fabrication of superhydrophobic graphene surfaces by means of two-beam laser interference (TBLI) treatment of graphene oxide (GO) films. Microscale grating-like structures with tunable periods and additional nanoscale roughness are readily created on graphene films due to laser induced ablation effect. Synchronously, abundant hydrophilic oxygen-containing groups (OCGs) on GO sheets can be drastically removed after TBLI treatment, which lower its surface energy significantly. The synergistic effect of micro-nanostructuring and the OCGs removal endows the resultant graphene films with unique superhydrophobicity. Additionally, dual TBLI treatment with 90° rotation is implemented to fabricate superhydrophobic graphene films with two-dimensional grating-like structures that can effectively avoid the anisotropic hydrophobicity originated from the grooved structures. Moreover, the superhydrophobic graphene films become conductive due to the laser reduction effect. Unique optical characteristics including transmission diffraction and brilliant structural color are also observed due to the presence of periodic microstructures. As a mask-free, chemical-free, and cost-effective method, the TBLI processing of GO may open up a new way to biomimetic graphene surfaces, and thus hold great promise for the development of novel graphene-based microdevices.

## 1. Introduction

Recent advances in biomimetic fabrication continue to stimulate the development of artificial materials and functional surfaces that possess fascinating properties similar to natural creatures.<sup>[1]</sup> The wettability control of solid surfaces is one of the most intensively investigated scientific fields.<sup>[2]</sup> Especially, triggered by the promising properties of superhydrophobic

H.-B. Jiang, Dr. Y.-L. Zhang, D.-D. Han, Dr. H. Xia,  
Prof. J. Feng, Prof. Q.-D. Chen, Prof. Z.-R. Hong,  
Prof. H.-B. Sun  
State Key Laboratory on Integrated Optoelectronics  
College of Electronic Science and Engineering  
Jilin University  
2699 Qianjin Street, Changchun 130012, China  
E-mail: yonglaizhang@jlu.edu.cn

Prof. H.-B. Sun  
College of Physics  
Jilin University  
119 Jiefang Road, Changchun 130023, China  
E-mail: hbsun@jlu.edu.cn



DOI: 10.1002/adfm.201400296

surfaces such as self-cleaning, anti-icing, anti-corrosion, and drag reduction,<sup>[3]</sup> great efforts have been devoted to the manufacturing of superhydrophobic surfaces based on a wide range of materials, including metal, metal oxides, polymer, carbon and even biomaterials.<sup>[4–7]</sup> It is well known that two factors govern the wettability of solid surfaces, one is geometrical microstructure, and the other one is chemical composition.<sup>[8,9]</sup> According to this basic principle, artificial superhydrophobic surfaces have been readily prepared by the combination of the as-mentioned two factors. Generally, the microstructuring with respect to hierarchical roughness could be realized with the help of various micronanofabrication techniques, represented by classical “bottom-up” approaches (e.g., Langmuir-Blodgett technique, Layer-by-layer assembly)<sup>[10–12]</sup> and “top-down” method (e.g., lithography, tip-technique);<sup>[13,14]</sup> while the tuning of surface energy with respect to the surface chemical composition usually resorts to covalent grafting of guest molecules (e.g., fluorinated silane)

or coating with low-surface-energy materials.<sup>[15]</sup> To date, despite the fact that artificial superhydrophobic surfaces have already revealed a cornucopia of both fundamental research and practical applications, continued efforts in endowing novel materials with unique dewetting property are still highly required to realize their structural and functional integrity.

Considering the fact that graphene exhibits outstanding electrical, optical, thermal, and mechanical properties,<sup>[16–18]</sup> which are promising for a wide range of scientific fields,<sup>[19,20]</sup> fabrication of micro-structured graphene films with unique superhydrophobicity is of great interest from the viewpoint of both experimental research and practical applications. Notably, the combination of graphene with superhydrophobicity would not only bring new opportunities for the development of novel graphene-based devices with remarkable performance, but also enable additional applications such as micro-droplet manipulation, anti-biofouling substrates, responsive switching and sensitive surface protection.<sup>[21]</sup> The attractive prospect of this dynamic field has motivated considerable efforts to develop superhydrophobic graphene films that feature refined control over surface wettability. For instance, Koratkar et al., successfully tune the

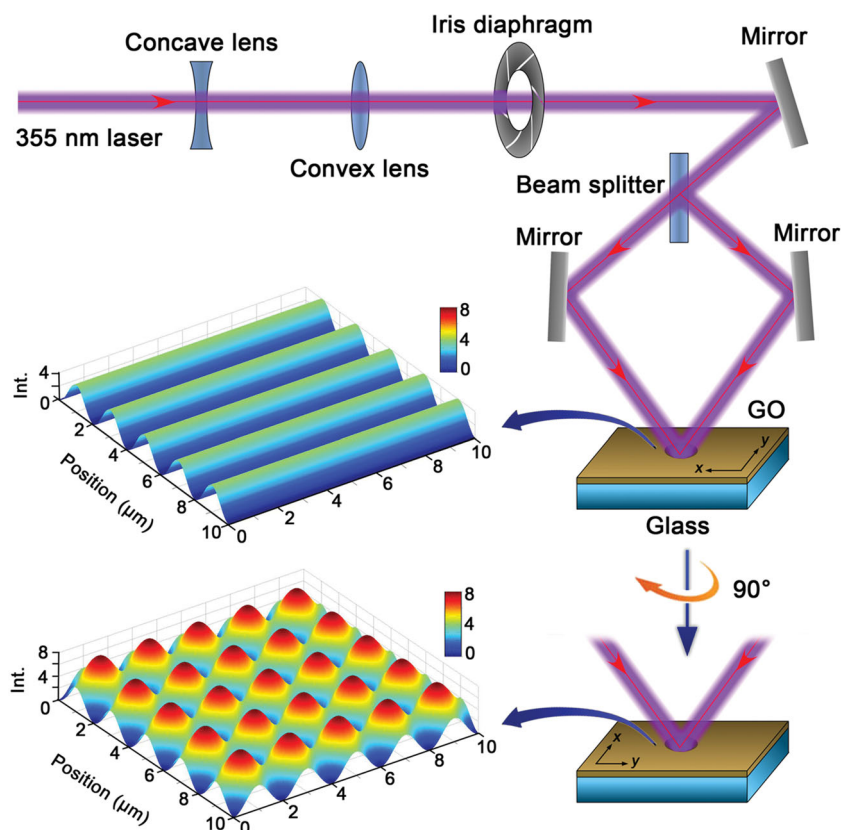


**Figure 1.** Schematic illustration of the fabrication of superhydrophobic graphene films by TBLI and dual TBLI treatment with 90° rotation. The insets are laser intensity distributions of TBLI and dual TBLI treatment with 90° rotation, which are calculated by Matlab.

surface wettability of thermally reduced GO from superhydrophobicity to superhydrophilicity by simply altering the solvents used for graphene dispersion.<sup>[22]</sup> The roughness effect in conjunction with the surface chemistry of the graphene sheets have been used to dramatically change the wettability of the RGO films. Kuo et al., reported a facile and inexpensive fabrication of superhydrophobic and superoleophilic graphene sponge using a simple dip coating method.<sup>[23]</sup> The porous structure of the sponge together with the microstructure of hydrophobic graphene nanosheets create a dually roughened surface, and thus alter its wettability from superhydrophilic to superhydrophobic property. Zhao et al., realized reversible control of the crumpling and unfolding of large-area graphene sheets on a PDMS sheet.<sup>[24]</sup> In this manner, the crumpled graphene films with self-organized hierarchical structures exhibit superhydrophobic property, which enable large-area and conductive graphene coatings with tunable wettability and transmittance. Additionally, superhydrophobic graphene films have also been fabricated through combined techniques such as suction filtration of chemically reduced GO,<sup>[25]</sup> template-directed chemical vapor deposition (CVD) growth of graphene foam,<sup>[26]</sup> and covalent graft of hydrophobic molecules on GO sheets.<sup>[27]</sup> However, in spite of these successful examples, the hierarchical roughness of the reported superhydrophobic graphene film usually comprises irregularly stacked multilayer graphene nanosheets and the folding of graphene wrinkles.<sup>[28]</sup> Currently, it is still

challenging to tailor the surface topography of graphene films through a biomimetic manner towards exquisite control of their surface wettability, since considerable difficulties arise when shaping the large but ultra-thin graphene sheets into periodic 2D or 3D microstructures.

Inspired from butterfly wings that exhibit both superhydrophobicity and brilliant structural color due to the presence of hierarchical roughness and the photonic crystal structures,<sup>[29]</sup> herein, we design and fabricate superhydrophobic graphene films with the help of two-beam laser interference (TBLI) technique. Periodically distributed grating-like microstructures could be easily created once the GO film was exposed to the interfered laser beams due to the laser induced ablation and reduction of GO sheets.<sup>[30]</sup> dual TBLI treatment with 90° rotation has been adopted for the construction of 2D grating-like structures on GO films, which effectively avoids the anisotropy in superhydrophobicity and conductivity. At the same time, the tuning of the surface chemical composition has been realized synchronously, since the laser treatment would remove most of the hydrophilic oxygen-containing groups (OCGs) on GO sheets, which renders the reduced GO (RGO) films both lower surface energy and higher conductivity. Consequently, the combined effects of microstructuring and OCGs removal endow the

resultant RGO film with both superhydrophobicity and brilliant structural color that mimic butterfly wings.

## 2. Results and Discussion

### 2.1. Optical System for the Fabrication of Superhydrophobic Graphene Films

Laser holography technique has been widely recognized as a powerful tool for rapid, mask-free, chemical-free and large-area micronanofabrication, especially in the case of 2D or 3D photonic crystals.<sup>[31,32]</sup> Previously, multi-beam laser interference (MBLI) induced micronanostructuring reported by our group<sup>[33,34]</sup> and others,<sup>[35,36]</sup> has already proved its value in the fabrication of biomimetic structures and devices that feature natural materials. In this work, we use TBLI to fabricate periodically structured graphene films in a biomimetic manner. **Figure 1** shows the schematic illustration of TBLI fabrication system. A frequency-tripled, Q-switched, single-mode Nd:YAG laser (Spectra-Physics) with the emission wavelength of 355 nm, frequency of 10 Hz, and pulse duration of 10 ns was employed for the processing. By using a beam splitter, the 355 nm laser beam was split into two equal-intensity beams, which were guided to interfere right on the surface of a GO film. The inset of **Figure 1** shows the laser intensity distribution

(LID) in the laser interference region. Generally, the intensity is constant along one direction, whereas the LID appears sinusoidal along its vertical direction. The highest intensity is calculated to be four times of each laser beam, and the minimum value is zero. When the GO film was exposed to the interfered laser beams, the surface morphology would be expected to be defined in a similar distribution due to the laser induced ablation and reduction effect, which means, in addition to the removal of OCGs, the GO sheets could be partially ablated in the region of high laser intensity, and survive in the low intensity region. It is well known that the parallel grooved microstructure would give rise to an obvious anisotropic dewetting property.<sup>[37]</sup> To avoid such anisotropy, the GO film could be rotated by 90° along the surface normal of the substrate, and additional TBLI treatment could be carried out in the perpendicular direction. As shown in the bottom of Figure 1, the LID reveals 2D grating structure in the case of dual TBLI; and the highest laser intensity is calculated to be eight times of each laser beam. In fact, the LID patterns could be precisely tuned by applying MBLI (e.g., four-beam laser interference, eight-beam laser interference) or multi-exposure of TBLI (e.g., thrice exposure of TBLI).<sup>[38,39]</sup> As proved in our previous work, up to 18-fold symmetry could be readily fabricated based on the negative photoresists.<sup>[40]</sup> However, in this work, we did not tune the LID patterns further, since more complex micropatterns would contribute little to the surface dewettability.

## 2.2. Tunable Periods of Graphene Microstructures

Taking advantage of TBLI technique, the periodicity of the grating could be precisely controlled by changing the angle of two laser beams, as shown in the following equation:

$$\Lambda = \frac{\lambda_F}{2\sin(\theta/2)} \quad (1)$$

where  $\Lambda$  is the period,  $\lambda_F$  is the laser wavelength and  $\theta$  is the angle between two beams. Figure 2a–h shows the SEM images of GO films with different periods fabricated by once TBLI. It could be clearly identified from the images that 1D grating-like structure formed on graphene films after TBLI treatment. By changing the angle between two laser beams, structured graphene films with periods in the range from 4 to 1  $\mu\text{m}$  have been readily fabricated. Figure 2h shows the comparison between the as-formed morphology and the LID. Obviously, in the region of high laser intensity, GO sheets have been partially ablated, whereas in the low intensity region, RGO survived and turnup graphene fragments formed on the top of the grating. Interestingly, additional layered nanostructures formed between the highest and the lowest laser intensity region, this could be attributed to the laser cutting effect

which makes edges of the interlayer RGO sheets expose to the surface. It is noteworthy that the formation of microscale grating-like structures together with the turnup graphene nano-fragments and nano-layer structures significantly increase the surface roughness, and therefore contribute to the superhydrophobicity. According to our experiments, the suitable laser power for the fabrication of hydrophobic graphene film is 0.2–0.4 W (before beam splitting). Further increase of the laser power would result in the ablation of more GO sheets, which decreases the surface roughness on the contrary; whereas the decrease of the laser power would lead to unobvious structures. In this work, all of the processing has been carried out under a moderate laser power of 0.4 W. Additionally, low magnified SEM image shows that the grating-like microstructures of the as-fabricated graphene film is very uniform over large area (Supporting Information, Figure S1). For comparison, the SEM image of pristine GO film reveals that the surface before TBLI treatment is very smooth (Supporting information, Figure S2), which indicates that TBLI is an effect processing technique for making periodic microstructures.

To quantitatively investigate the anisotropic superhydrophobicity of the microstructured graphene films with different periods, static water contact angle (CA) measurement has been carried out both along the grating direction and from the vertical direction. As shown in Figure 3, all of the microstructured graphene films show anisotropic hydrophobicity, generally with a CA value in the range of 120–153°. Considering the fact that the CA of the pristine GO film with a flat surface is only 70° (Figure S2, Supporting Information), the TBLI treatment induced micronanostructures are considered to be an essential factor to gain the hydrophobicity. Here, the period also plays a very important role, when the period was tuned from 1 to

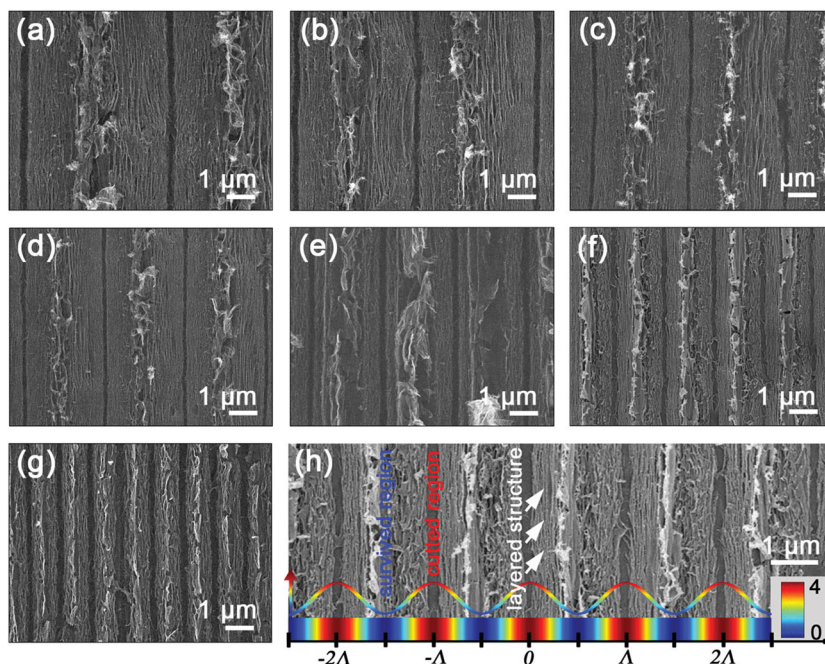


**Figure 2.** SEM images of TELI treated graphene films with different periods, a) 4  $\mu\text{m}$ , b) 3.5  $\mu\text{m}$ , c) 3  $\mu\text{m}$ , d) 2.5  $\mu\text{m}$ , e) 2  $\mu\text{m}$ , f) 1.5  $\mu\text{m}$ , g) 1  $\mu\text{m}$ . h) SEM image and the contrastive laser intensity distribution.

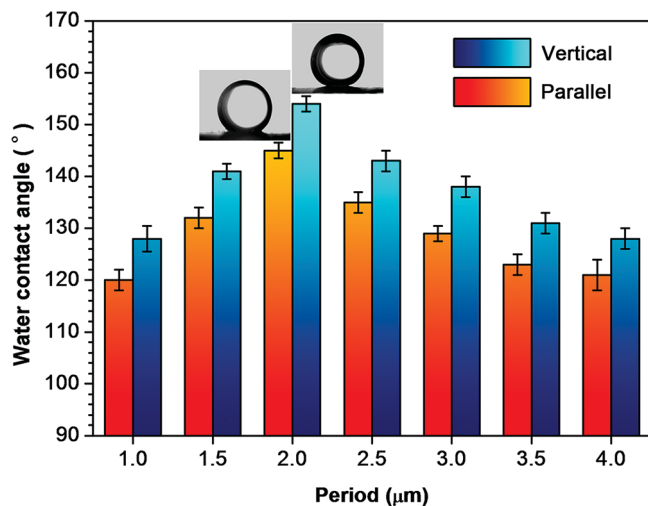


**Figure 3.** Dependence of the CA in both vertical and parallel directions of the grating structure on the grating periods from 1.0 to 4.0  $\mu\text{m}$ . The insets are the photographs of a water droplet on superhydrophobic graphene film with a period of 2.0  $\mu\text{m}$  viewed from vertical and parallel direction.

4  $\mu\text{m}$ , the CA changes with the periods, among which the graphene film with 2  $\mu\text{m}$  period shows the highest CA of  $\approx 153^\circ$ , reaching the superhydrophobic level. Additionally, the anisotropy of hydrophobicity is very obvious, the CA value along the parallel direction (observed from the vertical direction of grating) is generally 7–10° smaller than that along the vertical direction. The formation of such anisotropic hydrophobicity could be attributed to the macroscopic distortion of water drops which has been widely observed on some periodically grooved surfaces.<sup>[41]</sup>

### 2.3. From Anisotropic to Isotropic Superhydrophobicity

Despite the anisotropic superhydrophobicity shows great potential in water droplet manipulation and microfluidic devices, refined control over the dewetting property from anisotropy to isotropy is still highly desired in the consideration of the omnidirectional anti-water applications. In this work, to alter the structure/superhydrophobicity anisotropy, dual TBLI treatment with 90° rotation has been implemented to fabricate isotropic 2D grating-like structures on GO films. As shown in **Figure 4**, 2D micro-pillar arrays with square lattice structures have been successfully fabricated on the graphene films after dual TBLI treatment. Since the grooved graphene films with 2  $\mu\text{m}$  period show the strongest hydrophobicity, we fixed the period at 2  $\mu\text{m}$  in the case of dual TBLI. The CA of the resultant film measured from different direction is a constant value of 155°, which is similar with that of 1D grating-like structure (measured along the vertical direction). But obviously, it is isotropic. Magnified SEM images show that the 2D grating, the nano-layered structures on the side of the microgrooves, and the turnup graphene nano-fragments on the surface of each micro-pillar constitute the hierarchical roughness, which contributes to the surface superhydrophobicity (**Figure 4c,d**). It is worthy pointing out that the superhydrophobic graphene surfaces exhibit strong water adhesive property due to the presence of residual hydrophilic

OCCs. A water droplet could pin to the graphene surface firmly even when the surface was turned upside down (**Figure S3**, Supporting Information).

### 2.4. Characterization of Superhydrophobic Graphene Films

As mentioned previously, both the surface geometry and the chemical composition govern the surface dewetting property. In order to get further insight into the inherent mechanism of the formation of surface superhydrophobicity on the laser treated GO films, we investigate the surface topography and the chemical composition by atomic force microscope (AFM) and X-ray photoelectron spectroscopy (XPS), respectively. **Figure 5** shows the AFM images of the superhydrophobic graphene films. Notably, after TBLI and dual TBLI treatment, 1D and 2D grating-like structures could be clearly identified from the images, respectively. Interestingly, the patterns shown in the AFM image (**Figure 5a,d**) are quite similar with the LID patterns shown in **Figure 1**, and so do the SEM images (**Figure 2, 4**). In this regards, the formation of the periodically distributed sunken grooves is very obvious, it is due to the laser induced ablation and reduction of GO. Height profile along the white line of **Figure 5a** shows that the period is 2  $\mu\text{m}$ , and the height of the structure is  $\approx 500$  nm (**Figure 5b**). 3D transformed AFM images of 1D and 2D grating-like patterns reveal a visual observation of the surface topography.

In addition to the surface geometry, we also investigate the surface chemical composition of our GO films before and after TBLI treatments. **Figure 6** shows the C1s XPS spectra of pristine GO, TBLI treated RGO film and dual TBLI treated RGO films. The C1s peak could be simply deconvoluted into three peaks at 284.8, 286.9, and 288.8 eV, which could be attributed to C–C (nonoxygenated ring carbon), C–O (hydroxyl and epoxy carbon), and C = O (carbonyl), respectively. Notably, the content of oxygen atoms in pristine GO is as high as 31.5%, and the C/O atom ratio is only 2.2 (**Figure 6d**). After TBLI treatment,

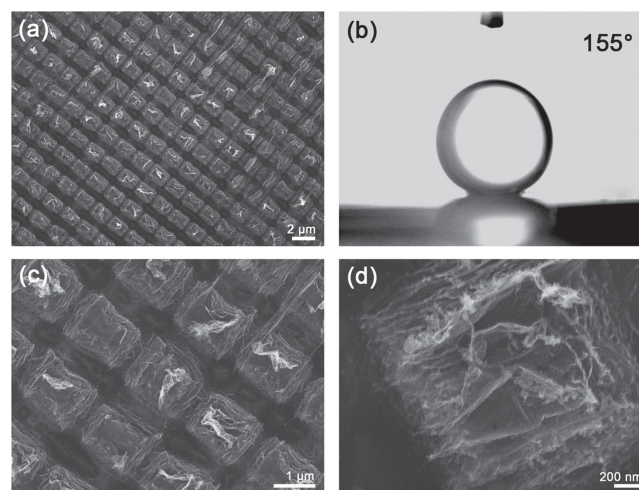


**Figure 4.** a) SEM images of superhydrophobic graphene film with 2D grating-like structures. The period is 2.0  $\mu\text{m}$ . b) Photograph of a water droplet on its surface, the CA is measured to be  $\approx 155^\circ$ . c,d) Magnified SEM images of 2D grating-like structures.

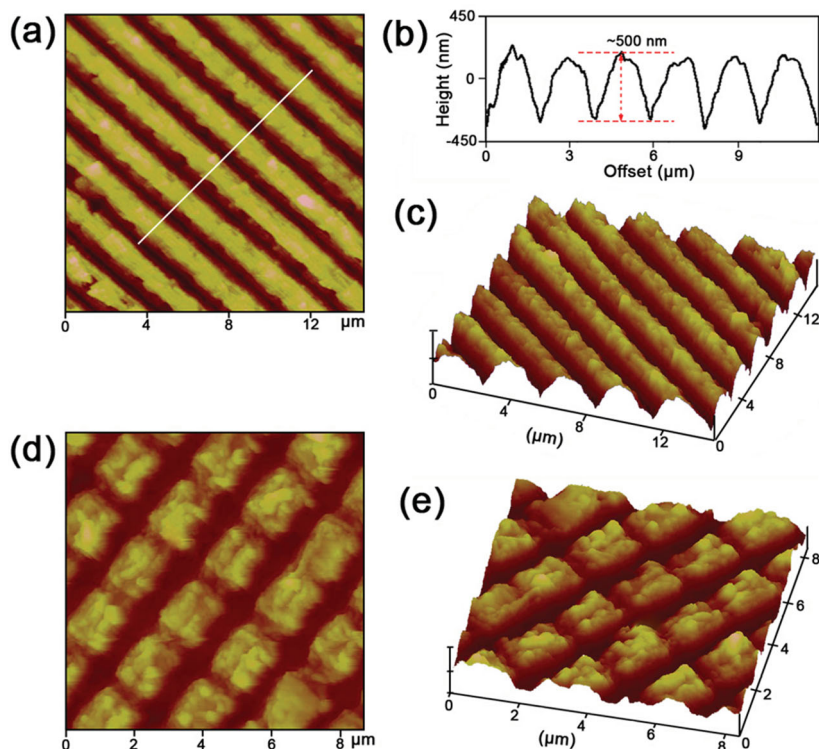


**Figure 5.** a–c) AFM image of superhydrophobic graphene films with 1D grating-like structures fabricated by TBLI. b) Height profile of the surface along the white line in (a). d,e) AFM image of superhydrophobic graphene films with 2D grating-like structures fabricated by dual TBLI treatment with 90° rotation.

the C–O and C = O peaks decreased significantly (Figure 6b), indicating the removal of OCGs on the GO sheets. According to the XPS results, the oxygen content of the TBLI treated graphene film decreased to 9.0%, and the C/O atom ratio increased to 10.2 accordingly. The significantly reduced oxygen contents

indicates that GO sheets have been effectively reduced to RGO during the TBLI induced ablation. It is noteworthy that the removal of hydrophilic OCGs would significantly reduce the surface energy, and thus contribute to the surface superhydrophobicity. Dual TBLI treatment would further decrease the oxygen content, as shown in Figure 6c. The oxygen content further decreased to 5.5%, and the C/O atom ratio increased to as high as 17.1, exhibiting a much higher reduction degree. Surface energies for both TBLI and dual TBLI treated graphene surfaces have been estimated according to Young's equation. Despite a simplified structure model has been used for the calculation, in which nanostructures have not been taken into account, the calculated results confirm that dual TBLI treatment would further decrease the surface energy, in good agreement with the XPS results (for calculation details, see Supporting Information).

To evaluate the structural change before and after TBLI, Raman spectra of GO and TBLI treated RGO films have been collected. As shown in Figure S4 (Supporting Information), the samples display two broad peaks at 1354 and 1599  $\text{cm}^{-1}$ , corresponding to D and G band, respectively. Generally, the G band peak is attributed to an  $E_{2g}$  mode of graphite associated with the vibration of  $sp^2$  bonded carbon atoms, whereas the D band peak is related to the vibrations of carbon atoms with dangling bonds in plane terminations of disordered graphite. After TBLI treatment, D and G band peaks show neglectable changes. Since the laser intensity in the interfered region is periodically distributed, we collect the Raman spectra alone

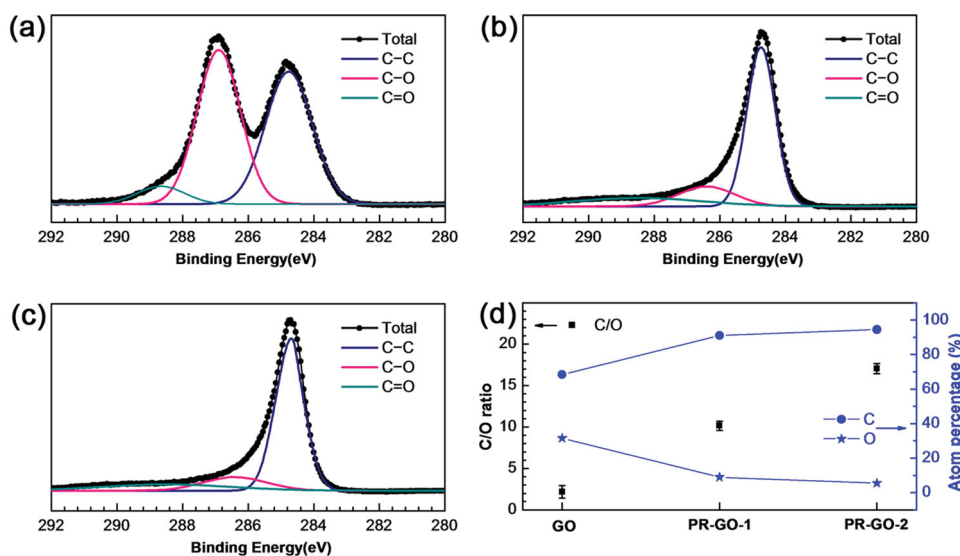


**Figure 6.** C1s XPS spectra of pristine a) GO and RGO films prepared by b) TBLI and c) dual TBLI treatment with 90° rotation. d) C/O atom ratios and the atom contents (C, O) of GO, and RGO films prepared by TBLI and dual TBLI treatment with 90° rotation.

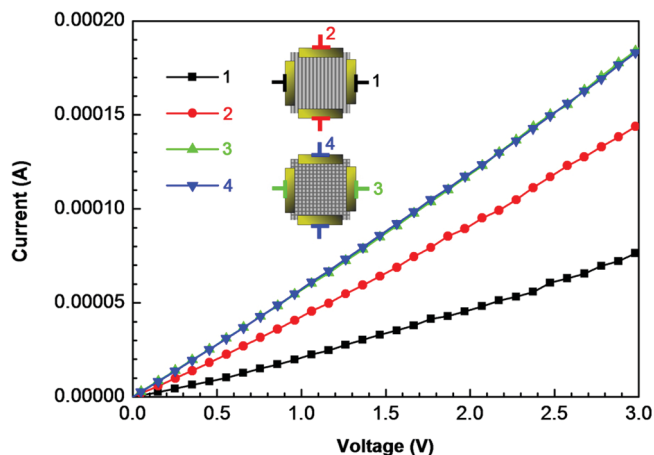


**Figure 7.**  $I$ - $V$  curves of RGO films with 1D and 2D grating-like structures measured on both vertical and parallel directions. The insets are schematic illustrations of the  $I$ - $V$  measurements.

the red line (Figure 7b,c). It could be clearly observed from the Raman maps that the D/G intensity ratios almost keep the same value. Theoretically, the removal of oxygen defects (OCGs) would render a much higher content of  $sp^2$  carbon, represented by a significantly increased G band peak. However, in the case of TBLI, the laser cutting induced ablation would bring abundant new defects on the edges of graphene sheets, which leads to the increase of D band peak. As a result of both “reduction” and “cutting” effects, the spectra show nonobvious changes.

## 2.5. Electrical and Optical Performance

Since the XPS spectra indicate that GO film have been effectively reduced after TBLI treatment, we also measure the electrical characteristics of the RGO films. In our work, the  $I$ - $V$  curves have been measured both along and against the 1D grating-like structure. As shown in Figure 7, as compared with GO which is isolating, the TBLI treated RGO film become conductive after laser reduction, the significant increase in conductivity could be attributed to the effective removal of the OCGs. However, considering the fact that TBLI treatment would cut RGO sheets into small pieces, and the some oxygen groups would survive in the low-laser-intensity region (Figure 1), the cutting effect together with the residual oxygen groups would decrease the conductivity to some extent. In this regards, the anisotropism in conductivity is very obvious. Resistance along the parallel direction (curve 2) of the grating is much smaller than that along the vertical direction (curve 1). This could be explained by the difference in reduction degree of the patterned RGO films, which is dominated by the LID (inset of Figure 1). In this regards, the bottom of the groove (cutted region, Figure 2h) is considered to be reduced more thoroughly, giving rise to much higher conductivity along the groove direction; whereas the survived region (Figure 2h) contains more OCGs residuals, leading to relative poor conductivity. This anisotropic conductivity could be effectively avoided by dual TBLI treatment with 90° rotation. After applying another TBLI treatment along the

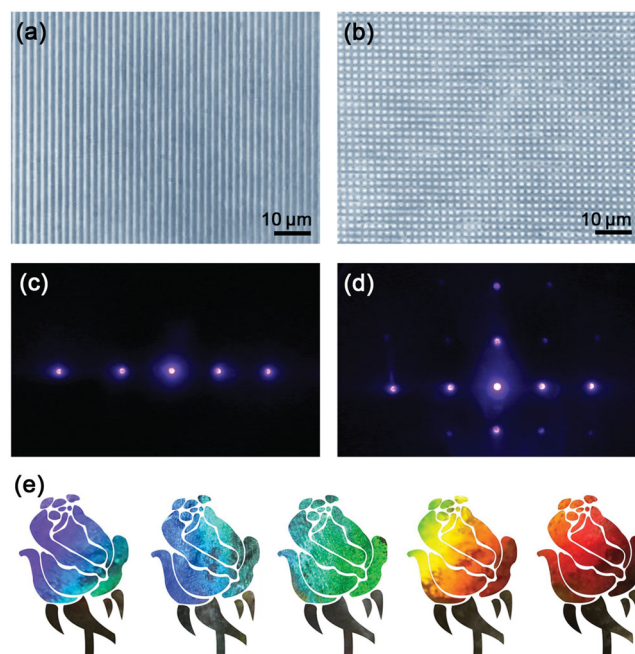


**Figure 8.** a) Optical images of graphene film with 1D grating-like structures, the period is 2.0  $\mu\text{m}$ . b) Optical images of graphene film with 2D grating-like structures, the period is 2.0  $\mu\text{m}$ . c,d) Diffraction spots fired by laser with wavelength of 405 nm on the RGO film with 1D and 2D grating-like structures. e) Structural color of the RGO films with 2D grating-like structures. The rose patterns are derived from pristine photographs the graphene film viewed from different angle by computer design.

vertical direction, RGO films with square lattice structures have been created, and the  $I$ - $V$  curves along the two directions (curves 3 and 4) confirm the isotropic conductivity.

Due to the scattering and diffraction of the grating-like structures, our superhydrophobic graphene films also exhibit unique optical characteristics. It could be clearly observed from the optical microscopic images that TBLI/dual TBLI treated graphene films show continuous and uniform 1D/2D grating-like structure in a large area (Figure 8a,b). Interestingly, when a 455 nm excitation light irradiates on the graphene films, uniform transmission diffraction spot could be clearly observed on the received screen (Figure 8c,d), indicating the uniform grating structures of the TBLI/dual TBLI treated graphene films. Additionally, when a beam of white light source irradiates on the graphene films, brilliant structural color could be clearly observed by naked eyes through a reflected mode. The iridescence could be attributed to the diffraction of the grating structures, expressed as the following equation:

$$m\lambda = d(\sin \theta_d - \sin \theta_i)$$

where  $m$  is the diffraction order,  $d$  is the period of the grating, and  $\theta_d$  and  $\theta_i$  are the diffraction and incident angles, respectively. By changing the viewing angle, light of a different wavelength diffracted, and beautiful colors separated ranging from purple to red could be observed due to the chromatic dispersion. We recorded such a structure color with a camera, filled them in a “Rose” template, as shown in Figure 8e.

### 3. Conclusion

Inspired from butterfly wings, periodically structured graphene films that feature superhydrophobicity and brilliant structural color have been successfully fabricated with the help of laser holography technique. TBLI and dual TBLI treatments of GO films gave rise to the formation of hierarchical roughness including microscale grating-like structures, graphene nanolayers and turnup graphene nano-fragments on the graphene surface due to the laser induced ablation and reduction effect. Besides, the laser treatments of GO also lead to drastic removal of hydrophilic oxygen groups on the GO sheets, which is confirmed by the results of C1s XPS. The micro-nanostructuring and the reduction of GO contributes to the tailoring of the geometrical microstructure and the tuning of the chemical composition of the graphene surface, respectively, giving rise to unique superhydrophobic properties that mimic butterfly wings. To avoid the anisotropy of superhydrophobicity in the case of 1D grooved structures, dual TBLI treatment with 90° rotation has been performed, graphene films with 2D grating-like structures show isotropic superhydrophobicity and electric property. Moreover, due to the presence of periodically distributed microstructures, the superhydrophobic graphene films also exhibit transmission diffraction property and brilliant iridescence, which could be directly observed by naked eyes. Taking advantage of these unique optical properties, it is reasonable to assume that novel optoelectronic devices, such as organic light emitting diodes (OLEDs) and organic solar cells (OSCs), would be developed based on the TBLI treated graphene films. Additionally, since graphene and graphene oxides have proved to be biocompatible scaffolds for human mesenchymal stem cells (hMSCs),<sup>[42]</sup> the micro-nanostructured graphene surface with tunable dewetting property may hold great potential in tissue engineering. We anticipate that the bioinspired graphene films would find broad application in various scientific fields, maybe beyond we can expect.

### 4. Experimental Section

**Materials and TBLI Fabrication:** GO was prepared from purified natural graphite (Aldrich, <150 μm) by following Hummers' method. The as-synthesized GO was dispersed into individual sheets in distilled water at a concentration of 3 mg mL<sup>-1</sup> with the aid of ultrasound. Glass substrates were cleaned with acetone, absolute ethanol, and deionized water, respectively. GO was spin-coated onto the glass substrates at 1000 rpm and dried to evaporate the solvent. Then, a frequency-tripled, Q-switched, single-mode Nd:YAG laser (Spectra-Physics) with about 10 ns pulse width ( $\lambda = 355$  nm; beam size  $\approx 9$  mm in diameter) was split into two beams with the same optical path length to the sample. Superhydrophobic graphene surfaces were fabricated by exposing the GO film to the interfered region of the laser beams.

**Characterization:** The CA measurements were made by using the Contact Angle System OCA 20 (DataPhysics Instruments GmbH, Germany) at ambient temperature. The CAs were measured with a water droplet of 4 μL. SEM images were obtained by using a field-emission scanning electron microscope (JSM-7500F, JEOL, Japan). X-ray photoelectron spectroscopy (XPS) was performed using an ESCALAB 250 spectrometer. Atomic force microscopy (AFM) images were obtained using a NanoWizard II BioAFM instrument (JPK Instruments AG, Berlin, Germany) in the tapping mode. Raman spectra were measured with a Renishaw Raman microscope using 514 nm wavelength laser.

### Supporting Information

Supporting Information is available from the Wiley Online Library or from the author.

### Acknowledgements

The authors would like to acknowledge National Basic Research Program of China. Grant Number: 2011CB013000; 2013CBA01700; NSFC. Grant Numbers: 61376123, 61008014 for support.

Received: January 27, 2014

Revised: February 20, 2014

Published online: April 22, 2014

- [1] K. Liu, L. Jiang, *Nano Today* **2011**, *6*, 155–175.
- [2] K. Liu, Y. Tian, L. Jiang, *Prog. Mater. Sci.* **2013**, *58*, 503–564.
- [3] Y. L. Zhang, H. Xia, E. Kim, H. B. Sun, *Soft Matter* **2012**, *8*, 11217.
- [4] S. N. Das, J. H. Choi, J. P. Kar, J. M. Myoung, *Appl. Surf. Sci.* **2009**, *255*, 7319–7322.
- [5] H. Y. Chen, J. C. Di, N. Wang, H. Dong, J. Wu, Y. Zhao, J. Yu, L. Jiang, *Small* **2011**, *13*, 1779–1783.
- [6] D. P. Hashim, N. T. Narayanan, J. M. Romo-Herrera, D. A. Cullen, M. G. Hahm, P. Lezzi, J. R. Suttle, D. Kelkhoff, E. Muñoz-Sandoval, S. Ganguli, A. Roy, D. J. Smith, R. Vajtai, B. G. Sumpter, V. Meunier, H. Terrones, M. Terrones, P. M. Ajayan, *Sci. Rep.* **2012**, *363*, 1–8.
- [7] T. Nakanishi, T. Michinobu, K. Yoshida, N. Shirahata, K. Ariga, H. Möhwald, D. G. Kurth, *Adv. Mater.* **2008**, *20*, 443–446.
- [8] L. Feng, S. H. Li, Y. S. Li, H. J. Li, L. J. Zhang, J. Zhai, Y. L. Song, B. Q. Liu, L. Jiang, D. B. Zhu, *Adv. Mater.* **2002**, *14*, 1857–1860.
- [9] X. M. Li, D. Reinhoudt, M. Crego-Calama, *Chem. Soc. Rev.* **2007**, *36*, 1350–1368.
- [10] K. Ariga, Y. Yamauchi, G. Rydzek, Q. Ji, Y. Yonamine, K. C. W. Wu, J. P. Hill, *Chem. Lett.* **2014**, *43*, 36–68.
- [11] K. Ariga, Y. Yamauchi, T. Mori, J. P. Hill, *Adv. Mater.* **2013**, *25*, 6477–6512.
- [12] Q. Ji, I. Honma, S. M. Paek, M. Akada, J. P. Hill, A. Vinu, K. Ariga, *Angew. Chem. Int. Ed.* **2010**, *49*, 9737–9739.
- [13] H. D. Yu, M. D. Regulacio, E. Ye, M. Y. Han, *Chem. Soc. Rev.* **2013**, *42*, 6006–6018.
- [14] J. Y. Cheng, C. A. Ross, H. I. Smith, E. L. Thomas, *Adv. Mater.* **2006**, *18*, 2505–2521.
- [15] D. Wu, J. N. Wang, S. Z. Wu, Q. D. Chen, S. Zhao, H. Zhang, H. B. Sun, L. Jiang, *Adv. Mater.* **2011**, *21*, 2927–2932.
- [16] K. S. Novoselov, A. K. Geim, S. V. Morozov, D. Jiang, Y. Zhang, S. V. Dubonos, I. V. Grigorieva, A. A. Firsov, *Science* **2004**, *5696*, 666–669.
- [17] Y. B. Zhang, Y. W. Tan, H. L. Stormer, P. Kim, *Nature* **2005**, *438*, 201–204.
- [18] S. Stankovich, D. A. Dikin, R. D. Piner, K. A. Kohlhaas, A. Kleinhammes, Y. Y. Jia, Y. Wu, S. T. Nguyen, R. S. Ruff, *Carbon* **2007**, *45*, 1558–1565.
- [19] K. S. Kim, Y. Zhao, H. Jang, S. Y. Lee, J. M. Kim, K. S. Kim, J. H. Ahn, P. Kim, J. Y. Choi, B. H. Hong, *Nat. Mater.* **2009**, *457*, 706–710.
- [20] P. Chen, J. J. Yang, S. S. Li, Z. Wang, T. Y. Xiao, Y. H. Qian, S. H. Yu, *Nano Energy* **2013**, *2*, 249–256.
- [21] Y. L. Zhang, Q. D. Chen, Z. Jin, E. Kim, H. B. Sun, *Nanoscale* **2012**, *4*, 4858.
- [22] J. Rafiee, M. A. Rafiee, Z. Z. Yu, N. Koratkar, *Adv. Mater.* **2010**, *22*, 2151–2154.
- [23] D. D. Nguyen, N. H. Tai, S. B. Lee, W. S. Kuo, *Energ. Environ. Sci.* **2012**, *5*, 7908.

- [24] J. F. Zang, S. Ryu, N. Pugno, Q. Wang, Q. Tu, M. J. Buehler, X. H. Zhao, *Nature* **2013**, *12*, 321–325.
- [25] J. Pu, S. H. Wan, Z. B. Lu, G. A. Zhang, L. Wang, X. Q. Zhang, Q. J. Xue, *J. Mater. Chem. A* **2013**, *1*, 1254.
- [26] E. Singh, Z. P. Chen, F. Houshmand, W. C. Ren, Y. Peles, H. M. Cheng, N. Koratkar, *Small* **2013**, *9*, 75–80.
- [27] Y. H. Xue, Y. Liu, F. Lu, J. Qu, H. Chen, L. Dai, *J. Phys. Chem. Lett.* **2012**, *3*, 1607–1612.
- [28] X. Q. Zhang, S. H. Wang, J. B. Pu, L. P. Wang, X. Q. Liu, *J. Mater. Chem.* **2011**, *21*, 12251.
- [29] J. Zi, X. D. Yu, Y. Z. Li, X. H. Hu, C. Xu, X. J. Wang, X. H. Liu, R. T. Fu, *Proc. Natl. Acad. Sci. U.S.A.* **2003**, *100*, 12576–12578.
- [30] J. N. Wang, R. Q. Shao, Y. L. Zhang, L. Guo, H. B. Jiang, D. X. Lu, H. B. Sun, *Chem. Asian J.* **2012**, *7*, 301–304.
- [31] Y. L. Zhang, L. Guo, S. Wei, Y. Y. He, H. Xia, Q. D. Chen, H. B. Sun, *Nano Today* **2010**, *5*, 15–20.
- [32] Y. Tian, Y. L. Zhang, J. F. Ku, Y. He, B. B. Xu, Q. D. Chen, H. Xia, H. B. Sun, *Lab Chip* **2010**, *10*, 2902–2905.
- [33] L. Wang, B. B. Xu, Q. D. Chen, Z. C. Ma, R. Zhang, Q. X. Liu, H. B. Sun, *Opt. Lett.* **2011**, *36*, 3305–3307.
- [34] L. Guo, H. B. Jiang, R. Q. Shao, Y. L. Zhang, S. Y. Xie, J. N. Wang, X. B. Li, F. Jiang, Q. D. Chen, T. Zhang, H. B. Sun, *Carbon* **2012**, *50*, 1667.
- [35] J. H. Moon, J. Ford, S. Yang, *Polym. Adv. Technol.* **2006**, *17*, 83–93.
- [36] L. G. Wang, L. Q. Wang, S. Y. Zhu, *Opt. Commun.* **2009**, *282*, 1088–1094.
- [37] D. Wu, J. N. Wang, S. Z. Wu, Q. D. Chen, S. Zhao, H. Zhang, H. B. Sun, L. Jiang, *Adv. Funct. Mater.* **2011**, *21*, 2927–2932.
- [38] Y. Jin, J. Feng, X. L. Zhang, Y. G. Bi, Y. Bai, L. Chen, T. Lan, Y. F. Liu, Q. D. Chen, H. B. Sun, *Adv. Mater.* **2012**, *24*, 1187–1191.
- [39] K. Kumar, K. K. Lee, J. Li, J. Nogami, N. P. Kherani, P. R. Herman, *Light: Sci. Appl.* **2014**, *3*, e175.
- [40] L. Wang, Z. H. Lv, X. F. Lin, Q. D. Chen, B. B. Xu, H. B. Sun, *IEEE J. Lightwave Technol.* **2013**, *31*, 276–281.
- [41] D. Xia, S. R. J. Brueck, *Nano Lett.* **2008**, *8*, 2819–2824.
- [42] W. C. Lee, C. H. Y. X. Lim, H. Shi, L. A. L. Tang, Y. Wang, C. T. Lim, K. P. Loh, *ACS Nano* **2011**, *5*, 7334–7341.